AFRL-VS-HA-TR-2007-1034

Observation of Tidal Effects on LWIR Radiance Above the Mesopause

Peter Wintersteiner

ARCON Corporation
260 Bear Hill Road
Waltham, MA 02451-1080

Scientific Report No. 2

7 March 2007

APPROVED FOR PUBLIC RELEASE; DISTRIBUTION UNLIMITED.

AIR FORCE RESEARCH LABORATORY
Space Vehicles Directorate
29 Randolph Road
AIR FORCE MATERIEL COMMAND
Hanscom AFB, MA 01731-3010

NOTICES

Using Government drawings, specifications, or other data included in this document for any purpose other than Government procurement does not in any way obligate the U.S. Government. The fact that the Government formulated or supplied the drawings, specifications, or other data does not license the holder or any other person or corporation; or convey any rights or permission to manufacture, use, or sell any patented invention that may relate to them.

This report was cleared for public release and is available to the general public, including foreign nationals. Qualified requestors may obtain additional copies from the Defense Technical Information Center (DTIC) (http://www.dtic.mil). All others should apply to the National Technical Information Service.

AFRL-VS-HA-TR-2007-1034 HAS BEEN REVIEWED AND IS APPROVED FOR PUBLICATION IN ACCORDANCE WITH ASSIGNED DISTRIBUTION STATEMENT.

//Signature//	//Signature//
JEREMY WINICK Contract Manager	ROBERT BELAND, Chief Battlespace Surveillance Innovation Center

This report is published in the interest of scientific and technical information exchange, and its publication does not constitute the Government's approval or disapproval of its ideas or findings.

REPORT DOCUMENTATION PAGE

Form Approved
OMB No. 0704-0188

1. REPORT DATE *(DD-MM-YYYY)*	2. REPORT TYPE	3. DATES COVERED *(From - To)*
7 March 2007	Scientific Report No. 2	08-01-2005 to 07-31-2006

4. TITLE AND SUBTITLE
Observation of Tidal Effects on LWIR Radiance Above the Mesopause

5a. CONTRACT NUMBER
FA8718-04-C-0031

5b. GRANT NUMBER

5c. PROGRAM ELEMENT NUMBER
612301

6. AUTHOR(S)
Peter P. Wintersteiner

5d. PROJECT NUMBER
2301

5e. TASK NUMBER
BD

5f. WORK UNIT NUMBER
A1

7. PERFORMING ORGANIZATION NAME(S) AND ADDRESS(ES)
ARCON Corporation
260 Bear Hill Road
Waltham, MA 02451-1080

8. PERFORMING ORGANIZATION REPORT NUMBER

9. SPONSORING / MONITORING AGENCY NAME(S) AND ADDRESS(ES)
Air Force Research Laboratory
29 Randolph Road
Hanscom AFB, MA 01731-3010

10. SPONSOR/MONITOR'S ACRONYM(S)
AFRL/VSBYM

11. SPONSOR/MONITOR'S REPORT NUMBER(S)
AFRL-VS-HA-TR-2007-1034

12. DISTRIBUTION / AVAILABILITY STATEMENT

Approved for Public Release; distribution unlimited.

13. SUPPLEMENTARY NOTES

14. ABSTRACT

An examination of CO_2 infrared limb radiance, directly measured by the SABER instrument aboard the TIMED satellite, reveals unusual structure in the region just above the mesopause, at tangent heights of ~95-110 km. Global coverage afforded by SABER makes it possible to investigate this behavior, which includes prominent regions with positive radiance gradients, as a function of latitude, local time, and season. The local-time dependence, in particular, suggests a role for atmospheric tides. Using a tidal model, Global Scale Wave Model, and our non-LTE ARC code, we modeled the 15 μm radiance. These calculations reproduced the main features of the global radiance structure, including the heights where positive gradients occur, and its variation with local time for different latitudes and seasons. The conclusion is that tidal perturbation of the temperature field in the lower thermosphere is directly responsible for the observed variability of the long-wave infrared limb radiance.

15. SUBJECT TERMS
Limb radiance, Radiance structure, Atmospheric tides, Mesospheric temperature inversion layer, TIL, SABER, MLT, CO_2, Infrared, Non-LTE, Diurnal, Semidiurnal, GSWM, ARC

16. SECURITY CLASSIFICATION OF:			17. LIMITATION OF ABSTRACT	18. NUMBER OF PAGES	19a. NAME OF RESPONSIBLE PERSON
a. REPORT	b. ABSTRACT	c. THIS PAGE			Jeremy Winick
U	U	U	UU	42	19b. TELEPHONE NUMBER *(include area code)*

Table of Contents

1. Introduction 1
2. Tidal Effects on LWIR Radiance 1
    2.1 Motivation 1
    2.2 Tides 2
    2.3 Radiance Structure and Atmospheric Temperature 3
    2.4 Global Patterns in SABER Data 5
    2.5 Modeling SABER Limb Radiance 6
        2.5.1 Tidal Fields 6
        2.5.2 Vibrational Temperature and Limb Radiance 7
    2.6 Model Results 8
    2.7 Comparisons with SABER Limb Radiance 8
    2.8 Discussion 10
    2.9 Summary 12

References 14

Figures 17

List of Figures

1.	SABER limb radiance from events of July 3, 2003	17
2.	Radiance profiles and retrieved temperature for two SABER events	17
3.	Average radiance distinguishing ascending and descending events	18
4.	Ascending/descending radiance differences throughout a yaw cycle	19
5.	Knee occurrence probabilities for January-March, 2004	20
6.	Knee tangent heights for January-March, 2004	21
7.	Knee occurrence probabilities for four yaw cycles in 2004	22
8.	Knee tangent heights for four yaw cycles in 2004	23
9.	Model predictions of temperature perturbations at the equator in March	24
10.	Tidally-perturbed profiles of temperature, atomic oxygen, and CO_2	25
11.	Predicted radiance for different local times, for April at the equator	26
12.	Predicted radiance for different local times for April at different latitudes	27
13.	Model-data radiance comparison for nighttime at the equator	28
14.	Model-data radiance comparison for daytime at the equator	28
15.	Model-data comparisons for various seasons, latitudes, and local times	29
16.	Model-data comparison, deviations of each from their respective means	30
17.	Model and data deviations from their means for different local times	31

1. INTRODUCTION

This Interim Scientific Report describes work that was undertaken according to the provisions of contract #FA8718-04-C-0031, during the second year in which it was in effect. The performance period was 1 August 2005 through 31 July 2006.

The subject of our report is a particular manifestation of the atmospheric tides, which are observed routinely in the mesosphere but not so easily above the mesopause, and whose characteristics are difficult to quantify in either case. We describe an analysis technique that directly demonstrates the existence and effect of tidal temperature perturbations in the lower thermosphere. The approach combines data from the SABER instrument [*Russell et al, 1999*], tidal modeling using Global Scale Wave Model [*Hagan, 1995; GSWM, 2004*], and our non-LTE Atmospheric Radiance Code (ARC) [*Wintersteiner et al, 1996*]. The basic idea is to show that high-altitude radiance profiles directly measured by SABER detectors have unusual characteristics that are explained only by tidal effects.

2. TIDAL EFFECTS ON LWIR RADIANCE

2.1. Motivation

The terrestrial upper mesosphere and lower thermosphere (MLT) have always been difficult regions to probe because *in situ* measurements can only be spaced irregularly and made infrequently, if at all. Satellite optical sensing offers the alternative of systematically studying the region, using retrieval algorithms to remotely determine temperature, pressure, and other quantities throughout its lower portions. Even this approach has suffered from relatively sparse coverage in the past, and from the difficulty of recovering temperature in a region where local thermodynamic equilibrium (LTE) does not hold. These problems were largely overcome with the 2001 launch of the TIMED (Thermosphere Ionosphere Mesosphere Energetics and Dynamics) satellite and the SABER (Sounding of the Atmosphere by Broadband Emission Radiometry) instrument that it carries.

SABER [*Russell et al, 1999*] is a ten-channel radiometer, one of four instruments aboard TIMED. Since early in 2002, it has been continuously scanning the limb between the ground and tangent heights of approximately 300 km, recording IR and NIR emissions from CO_2, H_2O, O_3, NO, OH, and O_2. Its nearly-continuous duty cycle, the high-inclination TIMED orbit, and sensitive detectors to enable high-altitude measurements combine to produce near-global coverage for many data products. Meanwhile, SABER CO_2 15 μm limb radiance is used to retrieve atmospheric temperature and pressure up to ~100 km, much higher than was previously possible. This is accomplished by a new non-LTE retrieval algorithm [*Mertens et al, 2001; 2002; 2004*].

Taking advantage of the wide spatial, temporal, and altitude coverage of retrieved products, we have used SABER data to study global characteristics of the mesopause, mesospheric thermal structure including inversion layers [*Wintersteiner and Cohen, 2005*], the OH layer [*Winick et al, 2006*], energy flow during auroral disturbances, and other MLT properties and phenomena. Some of this work incorporated interannual comparisons.

The work reported below involves atmospheric tides. The motivation was to address a question that has been the subject of inquiry since some of the earliest high-altitude rad-

iance measurements were made in the late 1970s [*Sharma and Nadile, 1981*]. The original puzzle was that 15 μm limb radiance from CO_2 was unexpectedly large for tangent heights above the mesopause. The explanation turned out to be the non-LTE nature of these emissions at high altitudes and the strong effect of atomic oxygen in exciting the bend-stretch states responsible for them [*Sharma and Wintersteiner, 1990; Wintersteiner et al, 1992*]. Nevertheless, many measured limb radiance profiles still defied explanation. Some radiance profiles appeared with positive gradients in the 95-110 km region, e.g. increasing radiance with increasing tangent height, whereas for others there was no hint of such a thing. One problem was that most of these "anomalous" positive-gradient profiles were impossible to simulate using temperature and constituent density profiles from standard climatologies. Another was that no explanation could be found for the apparent variability. Meanwhile, sparse data sets made it difficult to determine whether any systematic occurrence pattern existed. That, however, changed with the global coverage afforded by SABER.

We first addressed this problem by trying to determine the occurrence pattern for positive-gradient events. It soon became clear that they are correlated with latitude and local time (LT), in a complicated way that varies with the season. This suggests a tidal influence. [It also turns out that they are quite common. But for convenience we continue to describe them as "anomalous".] We turned to a state-of-the-art tidal model, Global Scale Wave Model [*GSWM, 2004*] to help us create model atmospheres that we could use to simulate tidal effects on radiance. These model atmospheres were used to initiate our own ARC non-LTE code [*Wintersteiner et al, 1992; 1996*], which enabled us to calculate the limb radiance for different cases. We are now able to show that tidal effects are not only sufficient to produce the positive radiance gradients, but they also explain their presence or absence.

2.2 Tides

Atmospheric tides are planetary-scale waves excited by various physical mechanisms. In the simplest picture, *in-situ* heating of the lower atmosphere due to the absorption of solar radiation produces upward-propagating disturbances that, in order to conserve energy, grow in amplitude with increasing altitude [*e.g., Hagan et al, 1999*]. This is accompanied by a downward progression of phase fronts with increasing time. The thermal and wind structure of the MLT region are both greatly perturbed. In particular, temperature variations of tens of degrees may occur in the upper mesosphere and lower thermosphere. These so-called "migrating" tides, locked to the apparent westward motion of the Sun, are diurnal, semidiurnal, terdiurnal, etc., waves according to the periodicity of each component. In each case, the zonal wavenumber is the inverse of the period. The diurnal migrating tide usually affects the MLT most strongly in equatorial regions, while the influence of the semidiurnal tide is strongest at midlatitudes.

A more complete picture also accounts for absorption by oxygen in the thermosphere itself [*Hagan et al, 2001*], as well as longitudinally-varying lower-atmosphere sources of heat that are not directly associated with the motion of the Sun. Among the latter, the most important is release of latent heat at the top of the troposphere due to deep convection in the tropics [*Hagan and Forbes, 2002; 2003; Oberheide et al, 2002*]. Forbes et al [*2006*] discuss this and other drivers for these "nonmigrating" tides, which may be eastward- or westward-propagating and have various wavenumbers. These authors analyzed

low- and mid-latitude SABER temperature data for a two-month period in 2002. They conclude that below 80 km the migrating tides dominate, but above that altitude a number of non-migrating components are clearly identified, with the so-called DE3 wave—the diurnal easterly wave of zonal wavenumber three—being especially prominent. Its genesis may be in the unusual austral stratospheric warming of 2002 [*Forbes et al, 2006*], but the analysis elucidates the complex interplay of tidal components and demonstrates their significance at high altitudes.

Tidal effects have been observed from the ground using optical emissions of various "layers" of the region: OH Meinel, OI green line, O_2 Atmospheric band, and the sodium doublet. Ground-based instruments [e.g., *Zhao et al, 2005; She et al, 2002, 2004*] have the advantage that they may be able to measure a particular volume throughout the diurnal cycle, although the difficulties of daytime measurements can be formidable. Satellite instruments provide much wider coverage but usually are restricted in their local time coverage. In the case of SABER, it requires approximately 60 days to acquire data for all accessible local times. As a result, any reconstruction of tidal fields from it can be affected by seasonal variations. Oberheide et al [*2003*] discuss difficulties involved in recovering such fields from satellite measurements, using SABER as the example.

As noted above, the tides manifest themselves as variations of the winds and temperature of the MLT region. Global Scale Wave Model [*GSWM, 2004*] is one means of quantifying these effects. GSWM is a state of the art model, and it is advantageous for our purposes because it provides general tables of tidal amplitudes and phases that can be used to construct perturbed temperature fields for our simulations. These tables from standard GSWM runs describe monthly zonal mean conditions for all latitudes and for altitudes up to ~125 km, for temperatures and winds, for the diurnal and semidiurnal migrating tides. The underlying calculations include all the primary sources of the migrating tides, but they exclude some of the longitudinally-dependent sources mentioned above. [GSWM can include many of those for special cases when lower-atmosphere conditions are specified in detail, but not for global overviews.] As such, the results provide an approximate measure of the tidal modulation of temperature, which is our main concern. With the most significant regular and repeatable tidal components available from this source, we proceeded with our program to model SABER 15 μm limb radiance.

2.3 Radiance Structure and Atmospheric Temperature

Figures 1a and 1b contrast six limb radiance profiles measured by SABER channel 3 on July 5, 2003, illustrating the variability that we remarked upon earlier. In Figure 1a, each of the three profiles has a region with an "anomalous" radiance gradient above the mesopause. Note, we also refer to these as "radiance knees" because of the shape of the curves. One sees that even among profiles with prominent knees there is considerable variability, not only in the altitude at which they occur but also in the intensity of the limb radiance. The latter varies by a factor of nearly three in the plots shown. Meanwhile, in Figure 1b, none of the three profiles has such a feature.

One also finds radiance profiles with positive gradients in the mesosphere. In Figure 2a, one of the two profiles falls off uniformly throughout the range of tangent heights, while the other has a knee near 110 km and another near 87 km. The lower of these is a direct reflection of a mesospheric temperature inversion layer (TIL) appearing near 87

km (shown in Figure 2b). The knee at 110 km, however, cannot so easily be associated with temperature. At these higher altitudes, LTE is a poor approximation, so its influence should be much diminished. Moreover, there are no obvious differences in temperature above the mesopause between the event with the knee and the event without one.

Notwithstanding these considerations, temperature may actually have a dramatic effect on 15 μm emissions. The primary excitation mechanisms for the emitting states there are radiative transfer and collisions with atomic oxygen. The former depends on conditions in the mesosphere below, where the photons being absorbed originate, but the latter reflects local conditions, in particular the CO_2 and O concentrations and the temperature. Even though the forward rate, k_o, for the process

$$CO_2(\nu_2) + O \underset{k_o'}{\overset{k_o}{\leftrightarrow}} CO_2(\nu_2 - 1) + O$$

is nearly independent of temperature, the reverse rate that is responsible for excitation depends strongly on it through the Boltzmann factor, because, for an energy difference E,

$$k_o' = (g'/g)\, k_o e^{-E/kT}$$

the g's being the statistical weights. The excitation rate is the product of three quantities: the densities of the two collision partners and the rate constant. Therefore, in a region where temperature increases sharply, as it does above the mesopause, one finds that, as altitude increases, if the exponential term rises faster than the product $[CO_2][O]$ falls, the emission rate rises also. One sees that the temperature gradient is a key parameter in determining this. One question that faces us, therefore, was whether the tides can modulate the temperature at such high altitudes, or (equivalently) modulate k_o', to an extent sufficient for producing radiance knees under certain conditions and not under others.With regard to Figure 2b, we note that because of good signal-to-noise ratios in the SABER 15 μm channels, the temperature-retrieval algorithm is stable up to ~125 km. However, the accuracy (3 K) intended for this data product is not achievable above 100 km because several quantities are uncertain, so the high-altitude results shown are not necessarily reliable. In fact, it is not known at all how accurate the retrieved temperature is at ~110 km. Therefore, although the temperature gradient appears to be greater for event 48 than it is for event 12 below 110 km—in agreement with our hypothesis—one must regard that fact as questionable evidence in its favor.

In the mesosphere, Figures 3 and 4 show what appears to be direct evidence, in a form not presented elsewhere, of tidal modulation of radiance. Channel-3 data were averaged for all events near the equator, 10^oN-10^oS, on particular days, distinguishing events on the ascending and descending portions of the orbits. Local time (LT) for each set of events varies slowly from day to day, but its difference at the equator remains fixed at ~9 hours. Meanwhile, the tide is dominated by its diurnal migrating component (12-hour period), especially near equinox when these observations were made. In Figure 3a one can easily distinguish radiance in the mesosphere at the two LTs. In Figure 3b, the oscillatory nature of the difference is highlighted. Figure 4 shows difference plots over a 60-day period, during which the local time of all observations shifts through ~12.5 hours.

Figure 4 is particularly suggestive of the diurnal migrating tide. The difference plots reveal a consistent vertical wavelength of ~22-25 km, an exponentially growing ampli-

tude in the mesosphere, and phase fronts that descend with LT at a rate of ~22 km per day. These are exactly the characteristics expected of this tidal component, and they apparently prevail even though the LT separation is ~9 hours rather than 12 and the data acquisition period is long enough for seasonal changes to be expected. Moreover, the perturbation is clearly seen well above the mesopause, in exactly the region we are investigating, even though its amplitude begins to diminish there. These are the original observations that led us to pursue this study. We note that at latitudes away from the equator where other tidal components are thought to exert greater influence, the structure becomes less organized—just as one would expect.

2.4 Global Patterns in SABER data

SABER data acquisition occurs within "yaw cycles" lasting approximately 60 days, the time it takes to view all accessible local times between the ascending and descending portions of the orbit. [LTs near local noon can never be observed because of detector sensitivity; a yaw maneuver is needed whenever the instruments point too close to the Sun.] The percent of events with anomalous radiance gradients above the mesopause for the January-March 2004 yaw cycle is shown in Figure 5a as a function of latitude and local time. The quantity plotted is the average over 3 degrees in latitude and 1 hour in LT. One immediately sees that, within this parameter space, there are regions where very few such events are found, and others where nearly all events have knees. At the equator, they occur preferentially after local noon, and a diurnal pattern is clearly evident. Near 30^o in each hemisphere, one finds semidiurnal patterns, as expected from tidal theory and as illustrated by latitude slices in plotted Figures 5b and 5c. Comparing the latter two, the maxima and minima occur at different LTs, perhaps because of winter-summer asymmetry. Some suggestions of diurnal and semidiurnal behavior at low- and mid-latitudes, respectively, are replicated in all periods for which we have analyzed SABER data.

We also find that the mean tangent heights at which the knees occur is correlated with latitude and local time. Figure 6 shows, in a format similar to that of Figure 5, mean tangent height for the same period of 2004. As with the occurrence likelihood, a diurnal pattern exists in the equatorial regions (see also Figure 6b). The range of mean altitudes is about 7 km, and they are not exactly correlated with the probability. Near 30^oN one again sees a semidiurnal pattern and (comparing Figures 5b and 6c) a lag between likelihood and mean altitude.

Figures 7 and 8 show the occurrence percentages and mean tangent heights, respectively, for most of the remainder of 2004. The effect of the polar summer temperature structure can be seen in Figures 7b and 8b. The occurrence probability north of ~65^o is large and independent of LT, and the mean altitude of the knees is less than ~101 km, lower than at other times and locations. This is apparently in accord with the low, cold mesopause, the rapid rise in temperature in the lower thermosphere, and the relative weakness of the tides at high latitudes. One also sees that the post-equinox periods (7a and 7d, 8a and 8d) are similar in the summer and winter hemispheres.

SABER yaw cycles cover the same periods each year, so it is possible to make interannual comparisons. Data that we have examined for 2002 and 2003 are generally similar to that shown for 2004. In particular, we find similar correlations with latitude and local

time, and similar suggestions of diurnal and semidiurnal behavior at the equator and mid-latitudes, respectively.

2.5 Modeling SABER Limb Radiance

The approach that we have adopted for predicting the 15 μm limb radiance is to (a) incorporate tide-induced local-time effects into model atmospheres; (b) calculate vibrational temperatures for the bend-stretch states, and the limb radiance; and (c) compare the latter with SABER data.

2.5.1. Tidal Fields

As noted earlier, we make use of results from the Global Scale Wave Model [*GSWM, 2004*] to incorporate local-time effects. Tables available on the GSWM web site provide the amplitudes and phases of the diurnal and semidiurnal tides for temperature and winds for each month of the year. We use the temperature tables, which list these quantities by latitude and altitude (~0-124 km.) The amplitudes and phases can be used to predict tidal temperature perturbations with respect to an assumed background atmosphere.

The process of constructing the model atmospheres needed for our calculations, task (a) above, starts with monthly-mean profiles, which are based on the NRL-MSIS00 climatology [*Picone et al, 2002*]. We wrote a driver program to set up repeated calls to MSIS using sequences of input parameters, perform suitable averages over one of them, and write out model atmospheres containing temperature, pressure, and all relevant constituent densities. MSIS can be set to produce zonal-mean profiles, eliminating all longitude and local-time effects. Our procedure is to simply calculate (for all latitudes of interest) these mean profiles for a range of days encompassing a single month and then average over that range. Since CO_2 is a critical component of our calculation that is not provided by MSIS, we include it by assuming a standard mixing ratio profile. The reason for using this approach is that GSWM also starts with MSIS monthly-mean atmospheres (supplemented by wind models and other data) as its background model. We made extensive checks to make sure that the mean profiles were consistent with previous results.

The second step was to calculate the tidal temperature perturbation, ΔT, for a given month as a function of altitude, latitude and local time. Our code interpolates the temperature amplitudes and phases for both modes onto a 1-km grid, and extrapolates them to ~145 km. Since the GSWM phases (given in hours) are piecewise continuous functions of altitude, and also may be quite irregular, it took considerable effort to develop a good algorithm for doing the interpolation. Extrapolating the amplitudes above 124 km required us to assume a damping factor to prevent exponential growth that would otherwise occur for certain situations. (Although speculative, the assumption we made is unlikely to affect the predicted radiance in the region of interest, which is below 115 km.) Given the amplitudes and phases on the proper grid, our code combines the diurnal and semidiurnal modes to generate ΔT. We thereby find that GSWM predicts perturbations approaching 90 K in the lower thermosphere for some months and latitudes. Smaller but quite significant values (~10-20 K) may be found for the upper mesosphere. In general, the latitude dependence is strong. The largest ΔTs occur near the equator and in narrow latitude bands near 30 degrees, whereas high-latitude perturbations are generally small. Figure 9 shows such results for March at the equator.

A third step is needed to combine the background atmosphere with the perturbations. Although the new temperature profiles are simply the background temperature plus ΔT, the process is complicated by the need to insure hydrostatic equilibrium in any valid model. It turns out that individual MSIS profiles, and therefore the monthly means that we start with, do not exactly satisfy this condition. It is therefore necessary to adjust the background atmosphere before including the tidal effect. We assume that the temperature profile is correct, and that the pressure (equivalently, the total number density) is correct at some particular point in the lower atmosphere. The pressure scale height can be calculated with confidence from the MSIS results, and it is straightforward to integrate it over the altitude range of interest. In the present instance, this modifies the density by at most ~1-2%. The greatest adjustment almost always occurs near 90 km, which may be a reflection of the algorithm used by MSIS to piece together its upper- and lower-atmosphere components. The choice of the lower-atmosphere "anchor" point has an even smaller effect on the results.

We then combine this slightly-adjusted background with the perturbation. The assumption, once again, is that the temperature profile ($T+\Delta T$) is correct. With large ΔTs, however, the hydrostatic readjustment of the background atmosphere now makes a much greater difference. Because of significant implied atmospheric heave, the scale height is no longer the same function of altitude as for the mean profile, particularly in the MLT region that is of greatest interest to us. We therefore assume that all the constituents' mixing ratios are fixed functions of pressure. That is, whatever the mixing ratio of $O(^3P)$ or any other constituent is at the pressure corresponding to, say, 95 km in the monthly-mean profile, it is the same at that pressure in the perturbed profile. Of course, that pressure may now occur at a significantly-different altitude. The scale height depends on temperature and gravity (functions of altitude, by assumption) and mean molecular weight (a function of pressure). It must be recalculated as a function of altitude in order to do the integration. This requires an iterative procedure, as there is an interdependence among the parameters in question. We run seven iterations, but there is very little change after the second one. This is the final step for producing sets of model atmospheres that can be used, one by one, in the next set of calculations.

Sample profiles in Figure 10 demonstrate the effect of tidal perturbations on temperature, and density of two constituents that are of great importance to our calculations. The slopes of the temperature profiles are notably different in the lower thermosphere.

2.5.2 Vibrational Temperature and Limb Radiance

The second major task, (b) in the brief outline given above, is to calculate the vibrational temperatures (T_v) of the bend-stretch states, and the limb radiance. This is accomplished using the ARC code [*Wintersteiner et al, 1996*] initialized with the new model atmospheres. For the sake of efficiency, we wrote scripts that allow us to run many sets of calculations automatically. We did the T_v calculations only for nighttime conditions, because each case then involves many fewer runs than it would for daytime. (Various daytime processes enhance the 15 μm radiance near 90 km, but only by a few percent.) These calculations are routine, having been performed by us many times in the past [e.g., *Wintersteiner et al, 1992*]. Even with the scripts and this simplification, however, it is a major task to simulate the full range of latitudes and local times, even for a single month of the year. In calculating the limb radiance, we used the SABER channel-3 filter.

We note that SABER temperature and pressure are derived from observed radiance, so retrieved products are not used at any place in our analysis. Rather, to avoid circular logic, only the MSIS climatology and model calculations from GSWM/ARC were used to simulate the radiance. All data comparisons are with the directly-measured radiance.

2.6 Model Results

Simulated limb radiance profiles were compiled at intervals of 2 hours in local time and 15 degrees in latitude, for several months. Figure 11 shows model results for April at the equator, a case for which tidal effects in the MLT are expected to be strong. The zonal mean simulated radiance shows no sign of a positive gradient, and very little change in slope, anywhere in the region depicted. [This is typical for a result based purely on climatology. It highlights the original problem we outlined in Section 2.1, namely that modeling results could not reproduce the radiance knees so frequently observed.] By way of contrast, exactly that sort of feature appears in the model results for some local times, but not others. For example, one sees that at LT ~ 8 hours there is no sign of a knee, in accord with the low probability in the SABER database shown for the equatorial region in Figure 7a. But for postnoon local times, positive gradients appear consistently, with the maximum radiance at varying tangent heights. In fact, starting at ~14 hours, the characteristic height appears to move downward with increasing local time through the night.

Figure 12 shows similar results for four other latitudes in the northern hemisphere. At 15^{o}N, a prominent knee is predicted only for one of the local times plotted and the structure in general is much weaker. At 30^{o}N and 45^{o}N, they show up in the morning hours, rather than postnoon as at the equator. At 60^{o}N (and more so at 75^{o}N, not shown) there is very little tidal modulation overall, in accord with theory, and no evidence of knees.

These results demonstrate convincingly that tidal influences are expected to be significant above the mesopause.

2.7 Comparisons with SABER Limb Radiance

To make model/data comparisons, we used SABER mean radiance profiles instead of individual events. To generate those, we averaged over 6-degree latitude bins and 1-hour LT bins. Local time changes by about 0.2 hours/day with the TIMED orbital precession, so data acquisition within each LT bin occurred over a period of about 5 days—except at high latitudes, when it is spread over longer periods. Data in different bins were therefore acquired sequentially rather than simultaneously during each yaw cycle, with results for two times (on the ascending and descending sides) obtained each day. Also, at the beginning and end of each cycle, there is some duplication of times near local midnight. For example, near the equator, data are acquired in the 0-1 hour LT bin on May 21-26 and on July 5-11, both periods falling within the north-looking May-July cycle each year. We were careful to avoid mixing data from separate ends of cycles.

Nevertheless, one generally expects seasonal changes to take place within the 60-day periods, possibly even within the 30-day months for which the simulations were done.

The model/data comparisons that we show, below, include direct juxtapositions of radiance profiles for different LTs. We also compare deviations of data from zonal-mean SABER radiance with deviations of model radiance (for different LTs) with zonal-mean model radiance. In neither case do the comparisons result in perfect agreement, for

reasons about which we speculate below. Even so, we find that tidal perturbations that substantially enhance or diminish the radiance above the mesopause are generally in accord in the data and the model results, producing or eliminating knees at varying tangent heights. Moreover, we confirm that zonal-mean radiance profiles contain no knees or positive gradients, either in the data or in the model.

We caution that the significance of "SABER zonal mean radiance", calculated by averaging over all LT bins after eliminating duplication at the beginning/end of the yaw cycles, is somewhat questionable. The idea is to approximate a diurnal mean to compare with LT-dependent results. But with no data at local noon, we cannot really calculate a 24-hour average properly. Even if we could, we would not be able to assign it to a single month because of the 60-day acquisition period. In spite of this, useful results can be obtained from the deviations calculated from it, as shown below.

Figure 13 presents a comparison of late-evening measured and model radiance. Acquisition periods for the SABER data are several-day blocks from April 11-16, 2004 (for events in the 20-21 hour LT bin) to March 27-April 1 (for the 23-24 hour period). Model calculations were for April. The most important result is that the shape of the radiance profiles is very well reproduced above ~90 km. The simulated knees appear at the correct tangent heights, and the variation of intensity with local time in that region—with larger radiance at later times—is also correct. As a result, we demonstrate not only that the tidal effects modulate the radiance above the mesopause, but also that these calculations correctly predict the extent of the changes.

Two other points stand out in Figure 13. One relates to the bumps in the data profiles near 80 km, which are caused by mesospheric temperature inversion layers. The inference that is drawn from their appearance in the mean profiles, which result from averaging over ~100 events, is that large TILs are ubiquious in the atmosphere this region. (In Figure 2, an example was shown for a single event.) There is a diurnal characteristic in this feature, as one sees by examining profiles for other local times, suggesting it also is tide-related. However, the model radiance fails to mimic it, and one concludes that the model tidal temperature amplitude is too small in the upper mesosphere for this case. This point is discussed further, below.

The other point is the overall underprediction of the radiance above ~80 km. This is also discussed in Section 2.8, but we note here that this is typical of our results, rather than exceptional. We never expected calculations based on MSIS climatology plus GSWM modeling to exactly reproduce SABER profiles, since there are known uncertainties and omissions in both. However, the discrepancies are consistently in one direction, and this deserves further consideration.

Figure 14 is like Figure 13, except the data and simulations were obtained for prenoon hours where few knees are found in the data. One sees that the model results confirm this expectation, while once again reproducing the shape of the data profiles but underpredicting them. These simulations use either March or April model input, to correlate with SABER data acquisition dates.

Figure 15 presents further comparisons, for mid and high latitudes. The model/data mismatches are similar to the equatorial case, but the general features of the data are in fact found also in the simulations. In (a) and (b), at southern midlatitudes in the fall, the

absolute agreement is better but the spread in model results is greater than that of the data. In (c) and (d), at northern midlatitudes in summer, one finds tidal modulations to be smaller but consistent between model and data. In (e) and (f), in the polar summer region, neither model nor data profiles change very much with local time. In none of these cases do we see the effect of large mesospheric TILs in the SABER data.

To strengthen the conclusion that tidal effects above the mesopause—that is, the perturbation of the radiance—are well represented despite the general underprediction, we show comparisons between deviations from monthly mean radiance of the model and data profiles. Figure 16a gives, in addition to plots for particular local times in the usual format, both the calculated mean radiance and the "SABER zonal mean radiance" mentioned earlier. In this case, we consider equatorial data from June and July, at local times near 2 hours, and as usual the model and data have the same general features. Figure 16b gives the percent deviations of the individual model and data profiles from their respective means. It shows that the tangent altitudes at which the individual profiles are greater or less than these means are nearly the same for data and model—that is, the signs of the deviations are the same. Moreover, the amounts by which this occurs are comparable in magnitude. For this case, it implies that the tidal perturbations imposed on the mean state are approximately correct, and that they are likely responsible for the appearance of knees at certain LTs and their absence at others.

Figure 17 makes comparisons like that shown in Figure 16b, but for late evening hours in the March-April time frame. One sees that ARC model radiance for the four LTs exceeds, or falls below, the monthly mean model radiance in much the same way the SABER radiance at corresponding times does with respect to its "zonal" or "diurnal" mean. In none of these cases do the model differences exactly reproduce the data differences, but these are typical results. One can see, by comparing the red and green curves representing March and April respectively, the extent of month-to-month variations in the modeled radiance. These variations are comparable to the model/data discrepancies.

2.8 Discussion

From the modeling results alone, we concluded that the tidal perturbation of kinetic temperature is sufficient to generate LWIR radiance structure of the size that is observed above the mesopause. With the data comparisons, we have shown that simulations predict radiance enhancements at nearly the right tangent heights, with approximately the right magnitude—the same being true, of course, for diminished radiance as well. This degree of agreement indicates that the tides are also necessary for explaining the results. It does not rule out a role for another physical mechanism, but we regard uncertainties in the present calculations as a plausible explanation for the discrepancies appearing in, for example, Figures 16b and 17.

The conclusions stated above refer to the perturbation of the radiance, the point being that the models correctly predict the changes induced by the tides. This work is based on a very simple idea, that temperature alone is responsible for inducing these changes. That in turn reflects the relatively straightforward processes (almost entirely radiative transfer and VT energy exchange) whereby excitation of the emitting CO_2 states is achieved. A separate important issue remains, however, and that is why the models systematically underpredict the data. The complete answer to that question remains elusive, but nothing

in the results we obtained indicates that the tidal model or the hydrostatic re-equilibration process is responsible. For example, the tidal model may have erroneous amplitudes or phases, but that should not induce a unidirectional offset, even factoring in changes such an error might cause in the equilibration. (The relatively minor effect of the latter can be seen in Figures 10b and 10c.) Rather, a more likely explanation is found in the background model atmospheres that we use to initialize the process.

NRL-MSIS00 [*Picone et al, 2002*] mean monthly profiles were our starting point, since those also initialized the tidal model [*GSWM, 2004*] that produced the tables we used. The atomic oxygen parameterization in this version of MSIS seems to produce less [O] at lower thermospheric altitudes than in previous versions. This would depress the modeled radiance, in comparison, but it takes a large increase in [O] to double the radiance, which is what would be necessary to produce model/data agreement in many cases. MSIS kinetic temperature could also be in error. Our present work demonstrates the sensitivity of the radiance to temperature, so this is a plausible source of error if profiles are systematically too cool at the mesopause and in the lower thermosphere. The MLT is surely the region with the fewest input data points for the MSIS parameterizations. But we know of no reports of temperature or [O] biases in this region, so this explanation must be regarded as speculative. The CO_2 profile that we inserted in all the monthly mean models is another possible source of systematic error. This is a standard profile scaled to 365 ppmv in the well-mixed region—up to 75 km in this model—and diminishing at higher altitudes. However, further uniform scaling to 380 ppmv would make little difference; it would be necessary to increase the density in the ~100-110 km region by many tens of percent.

Most likely, some combination of these factors is responsible for the problem we are considering. A further question, however, is the proper value of the rate constant for excitation of CO_2 by collisions with atomic oxygen. ARC uses the long-standing value of $\sim 6 \times 10^{-12}$ $cm^3/(mol\text{-}s)$ for this quantity [*Sharma and Wintersteiner, 1990*]. However, recent laboratory measurements [*Castle et al, 2006*] have produced a rate of $\sim 1.8 \times 10^{-12}$ $cm^3/(mol\text{-}s)$, less than a third as large. Incorporating such a small value in our calculations would further reduce the modeled radiance and increase the discrepancies.

A second issue, exemplified by Figure 13, is the failure of modeled radiance to reproduce positive-gradient radiance features that turn up at ~75-87 km, often but not exclusively in the equatorial region. We pointed out that such features result from the persistent presence of large inversion layers, like the 70-K TIL in Figure 2b. In fact, the correlation of mesospheric TILs and the migrating tides has been documented [e.g., *Meriwether et al, 1998*], including in our own studies of SABER data [*Winick et al, 2004; Wintersteiner and Cohen, 2005*]. However, no models, including GSWM, predict tidal amplitudes nearly as large as 70 K below 90 km (e.g., see Figure 9). Some reports indicate that GSWM amplitudes are too small to explain observations in that region [*She et al, 2002; 2004*]. Whether or not that is so, it is now accepted that tides alone are insufficient to produce very large TILs, which therefore require an amplifying mechanism [e.g., *Meriwether and Garrard, 2004*], such as coupling with breaking gravity waves, to explain their size. The implication, for our purposes, is that temperatures in some of our model atmospheres are lacking the proper structure below the mesopause, making it impossible to correctly calculate mesospheric radiance at certain times and places.

The atmospheric tide is a very complicated physical phenomenon. It would be difficult to incorporate all significant sources in a general model, especially longitude-dependent sources. One reason that nonmigrating modes are absent in the general tables we used is the requirement for very detailed input data to produce them. The same is true of the amplifying mechanisms to which we referred briefly. All in all, GSWM tables produce, at best, an approximation of the true tidal structure and therefore the MLT temperature at any particular time. That is true even if the zonal-mean initializing atmospheres from MSIS are very accurate.

Ignoring the general underprediction of SABER radiance, the imperfect correlation of model and data is best revealed in Figures 16b and 17. The discrepancies in altitude shown there, and in similar cases that we have examined, could be due to the phases of the GSWM migrating tides alone. The discrepancies in the deviations themselves at any tangent height could be due to a number of things, including the absent tidal modes. They could also be due to seasonal or interannual variations in the data. The latter would be revealed with a systematic year-to-year comparison of yaw cycles, but we have not done that yet. We note that Forbes et al [*2006*] conclude, from their examination of SABER data from 2002, that a wave-4 pattern—which is of course not modeled in GSWM results we used—appears with an amplitude of ~40-50 K near 110 km late that year. SABER temperatures are somewhat suspect at those heights, but a modulation of that size would certainly affect our results. They also suggest that this might have resulted in part from nonlinear interactions induced by the presence of an unusual southern-hemisphere stratospheric warming, which would be absent in data from other years.

Last of all, we note that seasonal variations cannot be extracted from SABER data requiring the full diurnal range in LT, because of the time required for data acquisition. To evaluate this, we directly compared nighttime data from the beginning and end of a few yaw cycles to see how much of a change occurs over the ~50-60 days. In some latitude bins, the knee occurrence probabilities are quite different, suggesting significant changes in the atmosphere or in the tides. This, like other factors we have mentioned, may well contribute to model/data discrepancies.

2.9 Summary and Conclusions

The work described above is, to our knowledge, the first attempt to address the question of how LWIR radiance is affected by the atmospheric tides in the decidedly non-LTE region above the mesopause. It answers the long-standing questions of what produces "radiance knees" there, and why the distribution of these features is so uneven.

Our hypothesis that studying atmospheric tides would be a fruitful approach to those questions arose from the rich radiance structure we observed in the SABER data. One observation was of ascending-descending radiance differences and the apparent progression of phase fronts, strongly suggestive of the diurnal tide, that they produce when viewed from day to day (Figure 4). Another was the latitude/LT dependence of the radiance knees themselves (Figures 5-8). In particular, both the occurrence rates and altitudes manifest diurnal patterns near the equator and semidiurnal ones at midlatitudes.

The approach we took was to model CO_2 15 μm radiance, incorporating tidal effects as best we could, in order to compare it with SABER channel-3 radiance. To do this, we began by creating monthly zonal mean (equivalently, diurnal mean) model atmospheres

from MSIS, generating tidal temperature perturbations using Global Scale Wave Model, and combining them to produce hydrostatically-equilibrated model atmospheres. We then used those to initialize our ARC code and calculate vibrational temperatures of the CO_2 bend-stretch states, and the corresponding limb radiance. We did this for local times throughout the day and for different latitudes and seasons. Finally, we created many sets of SABER limb radiance profiles, also broken out by local time, latitude, and season.

Direct comparisons of model results with these data showed that tidal effects are in fact responsible for the radiance knees observed in the lower thermosphere. The locations and altitudes of the knees are fairly well predicted by the model, despite known or suspected deficiencies in the physics and climatology incorporated in the calculations. One sees from our relatively simple approach that temperature, and temperature perturbations, are the driving force behind the radiance variability that is observed. Although it is well known that tidal temperature perturbations are significant in this region, most observations are of wind patterns rather than temperature. This is—to our knowledge—the first direct demonstration of temperature effects on radiance at those altitudes

The outstanding remaining question is what causes the underprediction of SABER limb radiance by our model. We discussed possible causes for this, including systematic under- or over-statement of input quantities from MSIS, and omission of nonmigrating tidal modes by GSWM. It has not been possible to determine conclusively the source of the discrepancy, but its effect does not invalidate the conclusions stated above.

Finally, although we did not address this point in our report, we note that the CO_2 LWIR emissions are the most important cooling mechanism in the altitude region under consideration. The ability to predict global infrared emission patterns, which is much improved by understanding the role played by atmospheric tides, should lead to better energy-balance calculations—in particular, the spatial and temporal variations in the balancing mechanisms. As such, it should result in improved global modeling of the MLT region.

REFERENCES

Castle, K.J., K.M. Kleissas, J.M. Rhinehart, E.S. Hwang, and J.A. Dodd, "Vibrational relaxation of CO2(v2) by atomic oxygen", *J. Geophys. Res.*, **111**, A09303, doi:10.1029/JA011736, 2006.

Forbes, J.M., J. Russell, S. Miyahara, X. Zhang, S. Palo, M. Mlynczak, C.J. Mertens, and M.E. Hagan, "Troposphere-thermosphere tidal coupling as measured by the SABER instrument on TIMED during July-September 2002", *J. Geophys. Res.*, **111**, A10S06, doi:10.1029/2005JA011492, 2006.

GSWM: Global Scale Wave Model, web.hao.ucar.edu/public/research/tiso/gswm/gswm.html, 2004.

Hagan, M.E., J.M. Forbes, and F. Vial, "On migrating solar tides", *Geophys. Res. Lett.*, **22**, 893-896, 1995.

Hagan, M.E., M.D. Burrage, J.M. Forbes, J. Hackney, W.J. Randel, and X. Zhang, "GSWM-98: Results for migrating solar tides", *J. Geophys. Res.*,**104**, 6813-6828, 1999.

Hagan, M.E., R.G. Roble, and J. Hackney, "Migrating thermospheric tides", *J. Geophys. Res.*, **106**, 12739-12752, 2001.

Hagan, M., and J.M. Forbes, "Migrating and nonmigrating diurnal tides in the middle and upper atmosphere excited by tropospheric latent heat release", *J. Geophys. Res.*, **107**(D24), 4754, doi:10.1029/2001JD001236, 2002.

Hagan, M. and J.M. Forbes, "Migrating and nonmigrating semidiurnal tides in the upper atmosphere excited by tropospheric latent heat release", *J. Geophys. Res.*, **108**(A2), 1062, doi:10.1029/2002JA009466, 2003.

Meriwether, J.W., X. Gao, V.B. Vickwar, T. Wilkerson, K. Beissner, S. Collins, and M.E. Hagan, "Observed coupling of mesosphere inversion layer to the thermal tidal structure", *Geophys. Res. Lett.*, **25**, 1479-1482, 1998.

Meriwether, J.W., and A.J. Gerrard, "Mesosphere inversion layers and stratosphere temperature enhancements", *Rev. Geophys.*, **42**(3), 8755, 1209/04/2003RG000133, 2004.

Mertens, C.J., M.G. Mlynczak, M. Lopez-Puertas, P.P Wintersteiner, R.H. Picard, J.R. Winick, L.L. Gordley, and J.M. Russell III, "Retrieval of mesospheric and lower thermospheric kinetic temperature from measurements of CO_2 15 μm Earth limb emission under non-LTE conditions", *Geophys. Res. Lett.*, **28**, 1391-1394, 2001.

Mertens, C.J., M.G. Mlynczak, M. Lopez-Puertas, P.P Wintersteiner, R.H. Picard, J.R. Winick, L.L. Gordley, and J.M. Russell III, "Retrieval of kinetic temperature and carbon dioxide abundance from non-local thermodynamic equilibrium limb emission measurements made by the SABER experiment on the TIMED satellite", *Proc SPIE*, **4882**, 162-171, 2002.

Mertens, C.J., F.J. Schmidlin, R.A. Goldberg, E.E. Remsberg, W.D. Pesnell, J.M. Russell III, M.G. Mlynczak, M. Lopez-Puertas, P.P. Wintersteiner, R.H. Picard, J.R. Winick, and L.L. Gordley, "SABER observations of mesospheric temperatures and comparisons with

falling sphere measurements taken during the 2002 summer MaCWAVE campaign", *Geophys. Res. Lett.*, **31**, L03105, doi:10.1029/2003GL018605, 2004.

Oberheide, J., M.E. Hagan, and R.G. Roble, "Sources of nonmigrating tides in the tropical middle atmosphere", *J. Geophys. Res.*, **107**(D21), 4567, doi:1029/2002JD002220, 2002.

Oberheide, J., M.E. Hagan, and R.G. Roble, "Tidal signatures and aliasing in temperature data from slowly precessing satellites", *J. Geophys. Res.*, **108**(A2), 1055, doi:1029/2002 JA009585, 2003.

Picone, J.M., A.E. Hedin, D.P. Drob, and A.C. Aikin, "NRLMSISE-00 empirical model of the atmosphere: Statistical comparisons and scientific issues", *J. Geophys. Res.*, **107**(A12), 1468, doi: 10.1029/2002JA009430, 2002.

Russell, J.M. III, M.G. Mlynczak, L.L Gordley, J. Tansock, and R. Esplin, "An overview of the SABER experiment and preliminary calibration results", *Proc. SPIE*, **3756**, 277-288, 1999.

Sharma, R.D., and P.P. Wintersteiner, "Role of carbon dioxide in cooling planetary thermospheres", *Geophys. Res. Lett.*, **17**, 2201-2204, 1990.

Sharma, R.D., and R.M. Nadile, "Carbon dioxide (ν_2) radiance results using a new nonequilibrium model", AIAA paper 81-0426, 19th AAIA Aerospace Sciences Meeting, 1981.

She, C.Y., S. Chen, B.P. Williams, Z. Hu, D.A. Kreuger, and M.E. Hagan, "Tides in the mesopause region over Fort Collins, Colorado (41°N, 105°W) based on lidar temperature observations covering full diurnal cycles", *J. Geophys. Res.*, **107** (D18), 4350, doi: 10.1029/2001JD001189, 2002.

She, C.Y., T. Li, R.L. Collins, T. Yuan, B.P. Williams, T.D. Kawahara, J.D. Vance, P. Acott, and D.A. Kreuger, "Tidal perturbations and variability in the mesopause region over Fort Collins, CO (41N, 105W): Continuous multi-day temperature and wind lidar observations", *Geophys. Res. Lett.*, **31**, L24111, doi:10.1029/2004GL021165, 2004.

Winick, J.R., P.P. Wintersteiner, R.H. Picard, C.J. Mertens, M.G. Mlynczak, M.E. Hagan, W.E. Ward, J.M. Russell, and L.L. Gordley, "Global occurrence statistics of mesospheric inversion layers obtained from SABER temperature profiles," *Eos Trans. AGU*, **85**(46), Fall Meet. Suppl., Paper SA34A-06, 2004.

Winick, J.R., R.H. Picard, P.P. Wintersteiner, D. Esplin, M.J. Taylor, I. Azeem, M.G. Mlynczak, J.M. Russell III, L.L. Gordley, and G. Crowley, "Interannual variability of OH Meinel emission as determined from SABER limb measurements at 1.6 and 2.0 microns", *EOS Trans AGU*, **87**(47), Fall Meeting Supplement, SA21-0224, 2006.

Wintersteiner, P.P., R.H. Picard, R.D. Sharma, J.R. Winick, and R.A. Joseph, "Line-by-line radiative excitation model for the non-equilibrium atmosphere: Application to CO_2 15 μm emission", *J. Geophys. Res.*, **97**, 18083-18117, 1992.

Wintersteiner, P.P., A.J. Paboojian, and R.A. Joseph, "Studies of non-LTE atmospheric emissions: modeling and data analysis", Philips Laboratory Technical Report, PL-TR-96-2226, 1996.

Wintersteiner, P.P, and E. Cohen, “Observations and modeling of the upper mesosphere: Mesopause properties, inversion layers, and bores”, Air Force Research Laboratory Technical Report, AFRL-VS-HA-TR-2005-1162, 2005.

Zhao, Y., M.J. Taylor, and X. Chu, “Comparison of simultaneous Na lidar and mesospheric nightglow temperature measurements and the effects of tides on the emission layer heights”, *J. Geophys. Res.*, **110**, D09S07, doi:10.1029/2004JD005115, 2005.

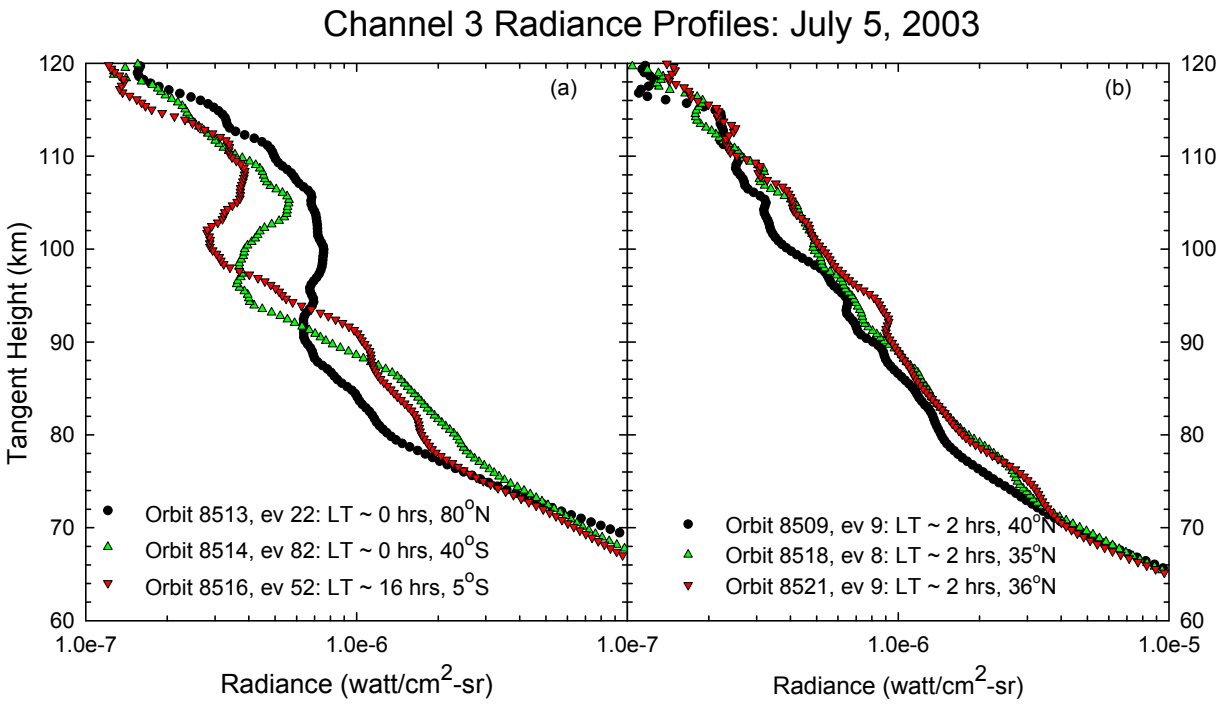

Figure 1. SABER limb radiance from events of July 3, 2003. (a) Three cases with positive gradients at different heights above 90 km; (b) Three cases with no such features

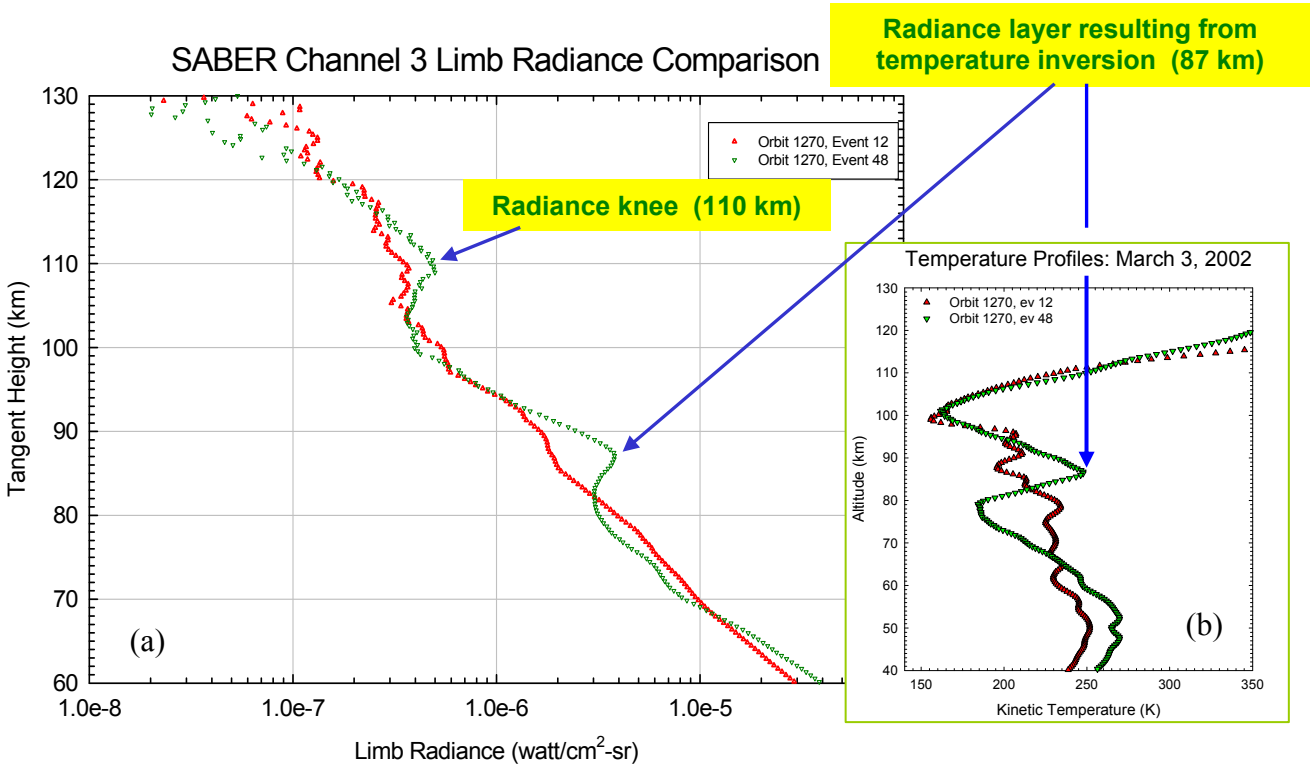

Figure 2. (a) SABER channel-3 radiance profiles from March 3, 2002. Event 12, at 48°N, has little radiance structure whereas event 48, at 7°S, has "knees" near 110 km and 87 km. The 87-km layer was caused by a mesospheric temperature inversion layer (TIL). (b) Retrieved temperature for these two events.

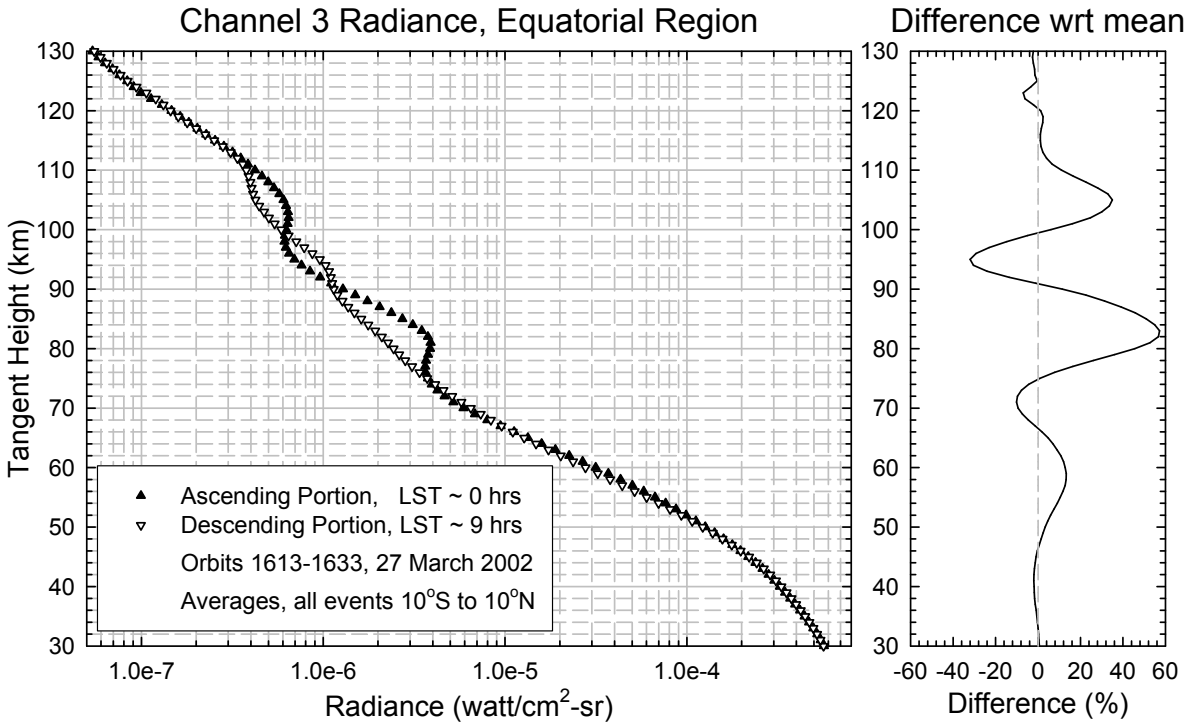

Figure 3. (a) Average channel-3 radiance for 10°N-10°S, 27 March 2002, distinguishing ascending (LT~0.1 hrs) and descending (LT~9.0 hrs) portions of the orbits. (b) The radiance difference, expressed as a percentage of the mean.

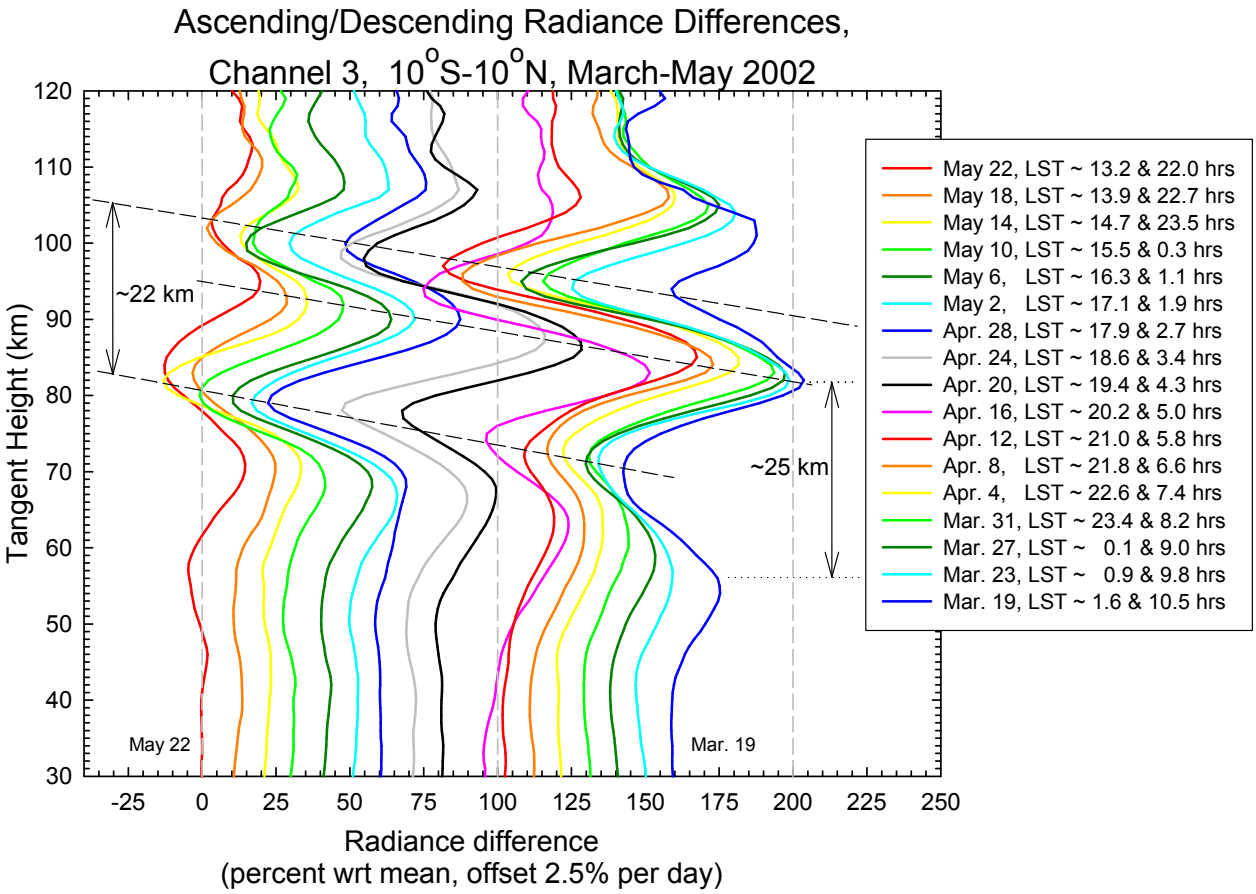

Figure 4. Ascending/descending radiance differences from SABER channel 3. Data as in Figure 3b, but for every fourth day during a yaw cycle commencing at vernal equinox 2002, reveal a quasiperiodic disturbance with a vertical wavelength of ~22-25 km. Slopes of the superposed lines are equivalent to a change of ~11.5 km/12.5 hrs of local time, or 22 km/day.

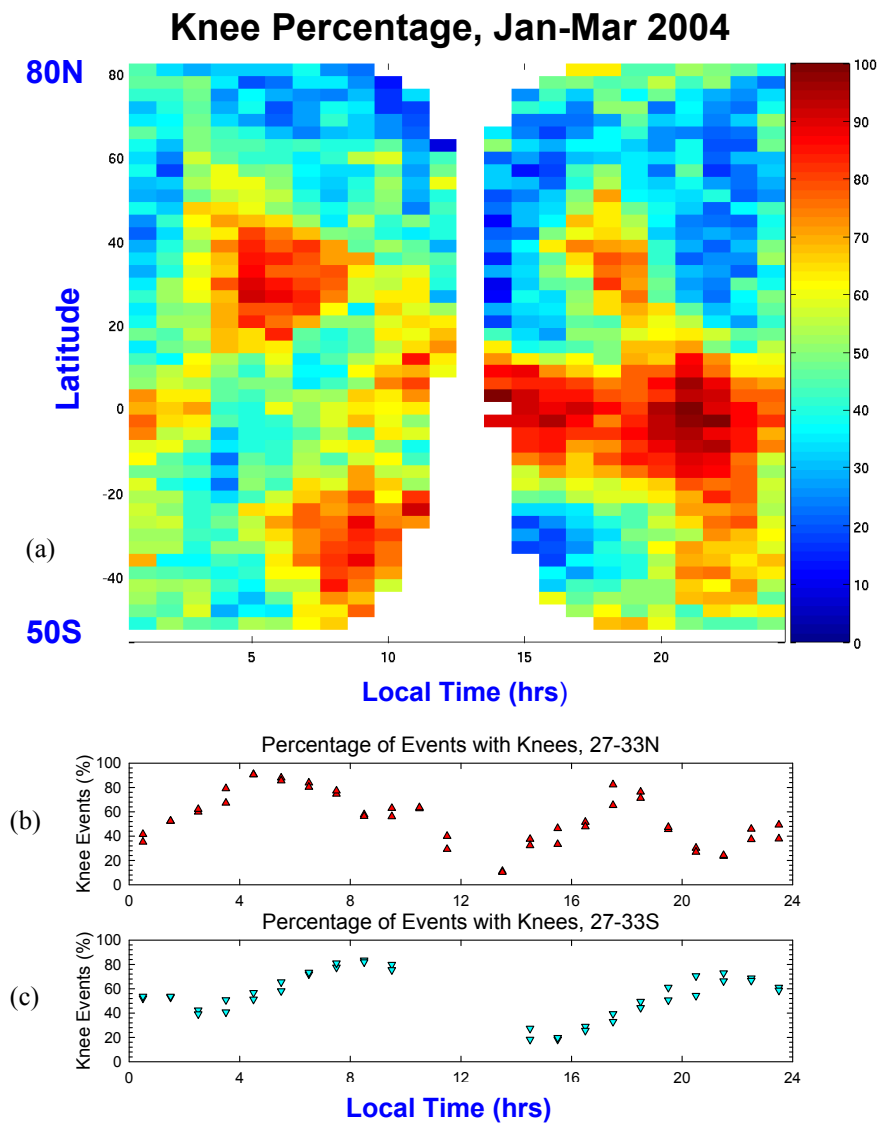

Figure 5. Occurrence pattern for Jan. 15-Mar. 19, 2004. (a) The percentage of events with radiance knees above 90 km, for the full accessible range of latitudes and local times; (b) the percentage near 30°N; (c) the percentage near 30°S.

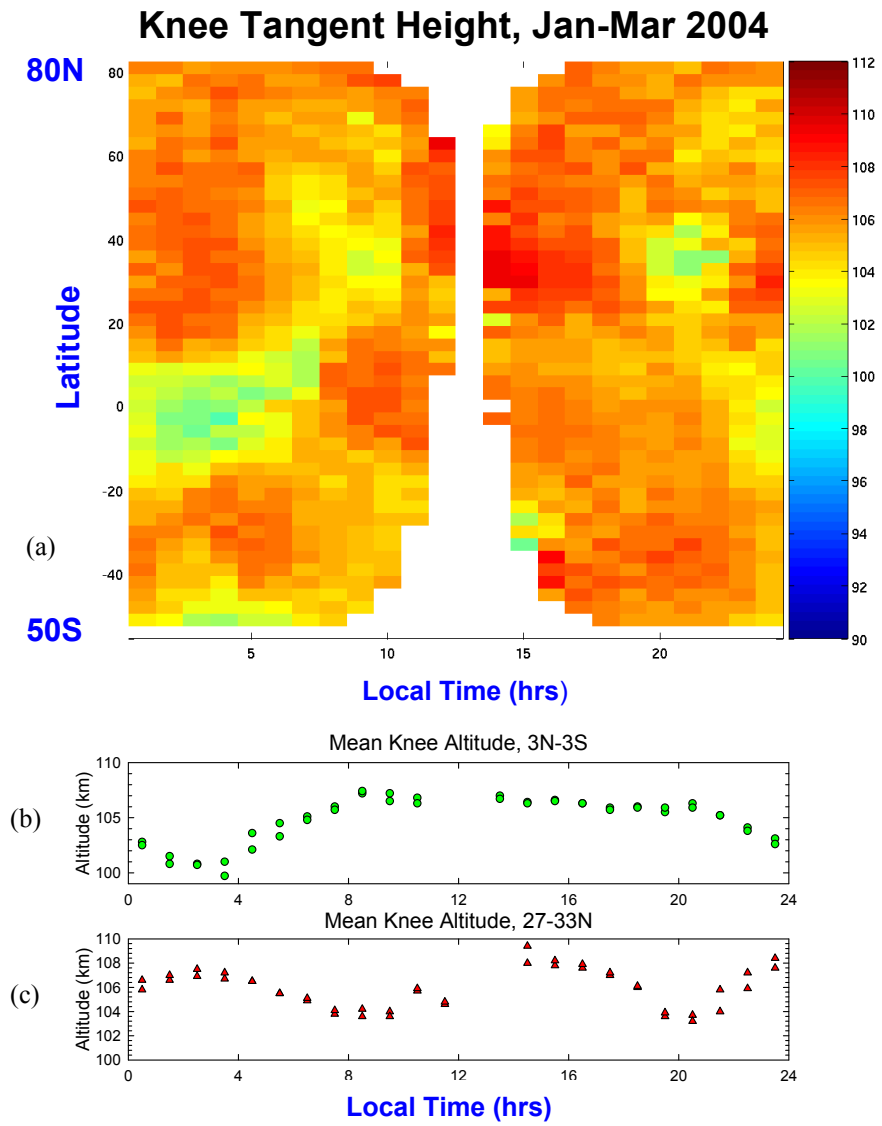

Figure 6. Mean tangent height for radiance knees, Jan. 15-Mar. 19, 2004. (a) Tangent altitudes for all events; (b) the altitudes near the equator; (c) the altitudes near 30°S.

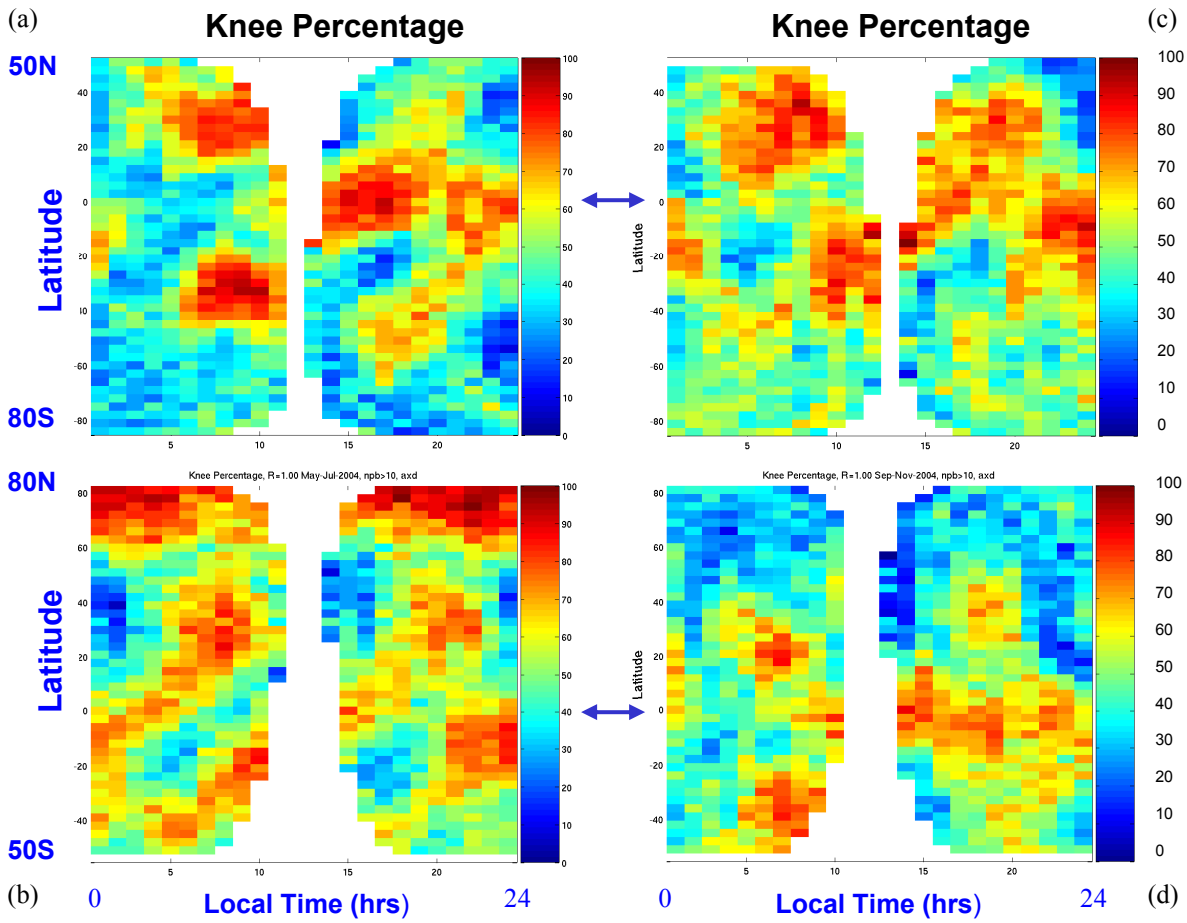

Figure 7. Knee occurrence percent, as in Figure 5a, for four other yaw cycles of 2004. (a) March-May; (b) May-July; (c) July-September; (d) September-November. The equator is indicated by the blue arrows.

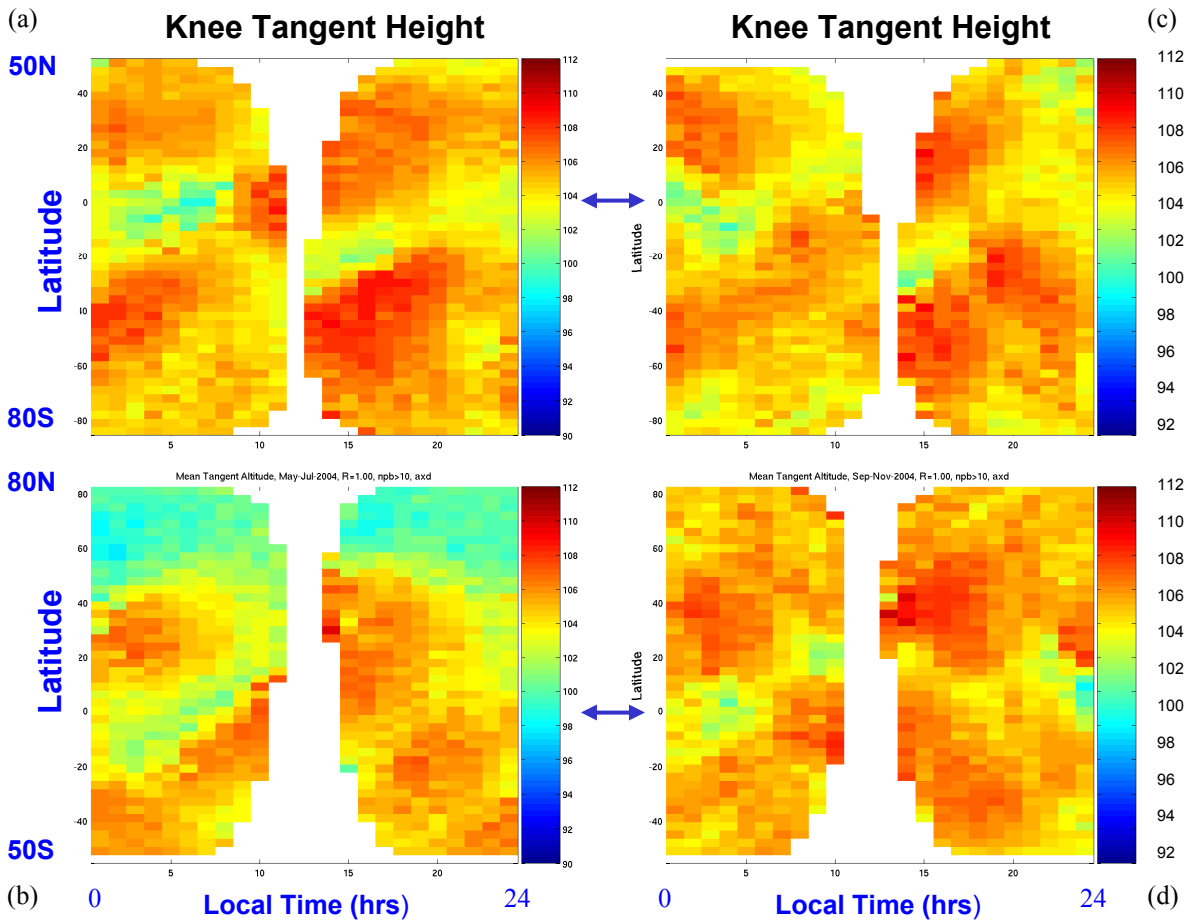

Figure 8. Knee tangent heights, as in Figure 6a, for four other yaw cycles of 2004. (a) March-May; (b) May-July; (c) July-September; (d) September-November. The equator is indicated by the blue arrows.

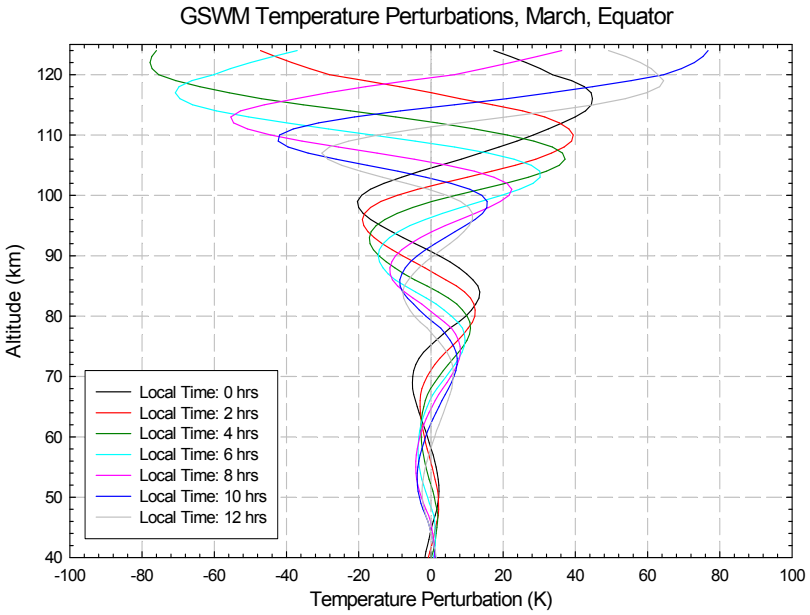

Figure 9. GSWM predictions of temperature perturbations for March at the equator, for different local times.

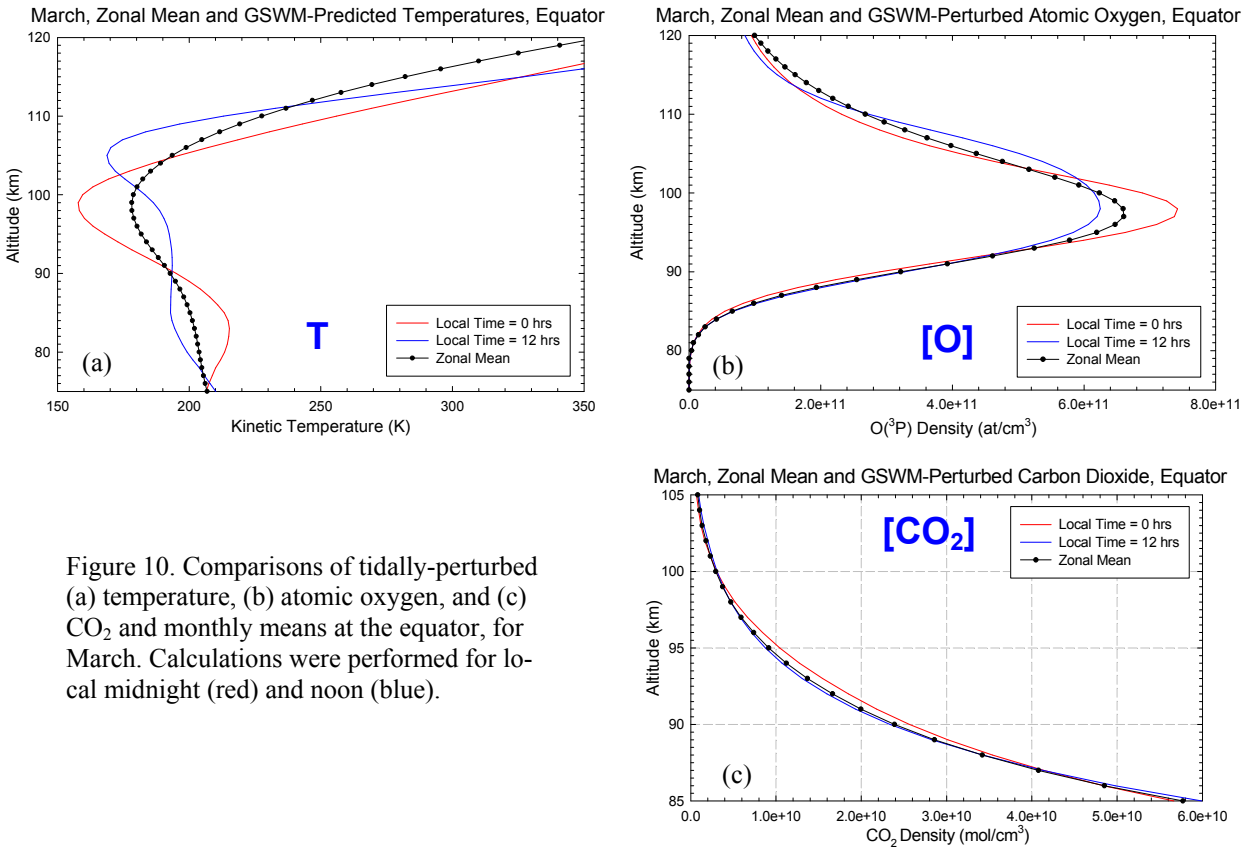

Figure 10. Comparisons of tidally-perturbed (a) temperature, (b) atomic oxygen, and (c) CO_2 and monthly means at the equator, for March. Calculations were performed for local midnight (red) and noon (blue).

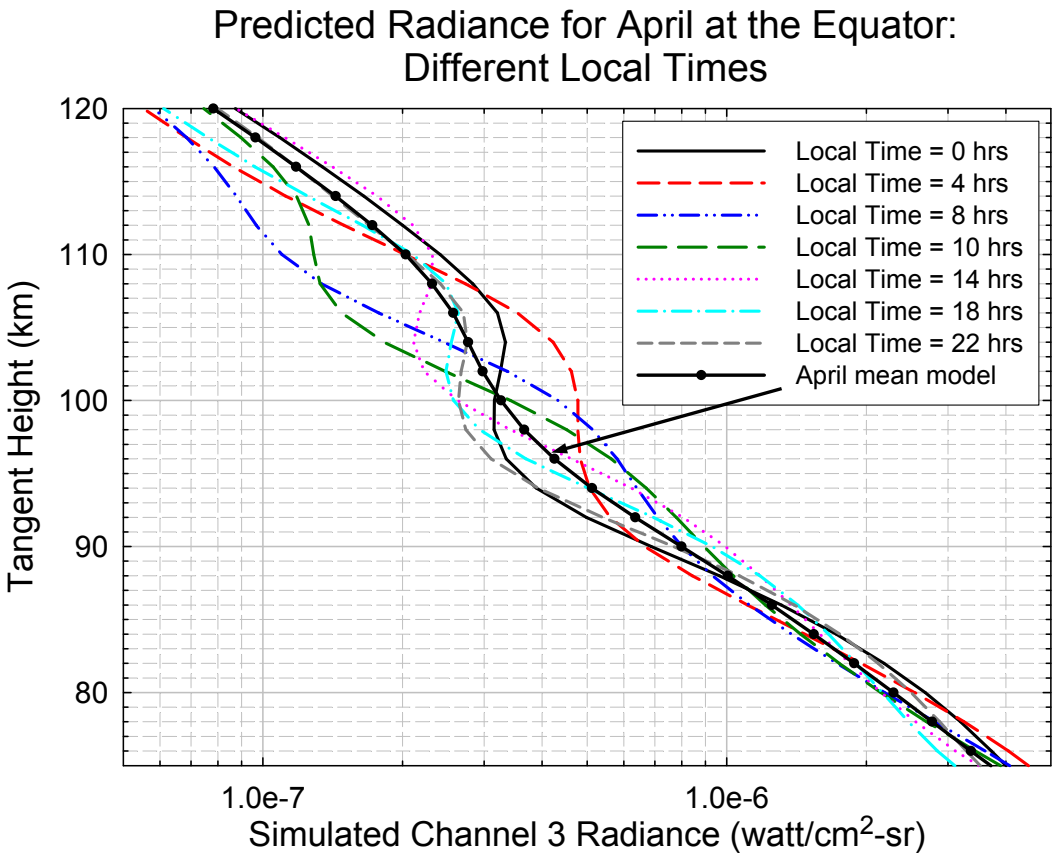

Figure 11. Predicted radiance at the equator in April for different local times, from GSWM/ARC modeling. Zonal mean radiance is also shown.

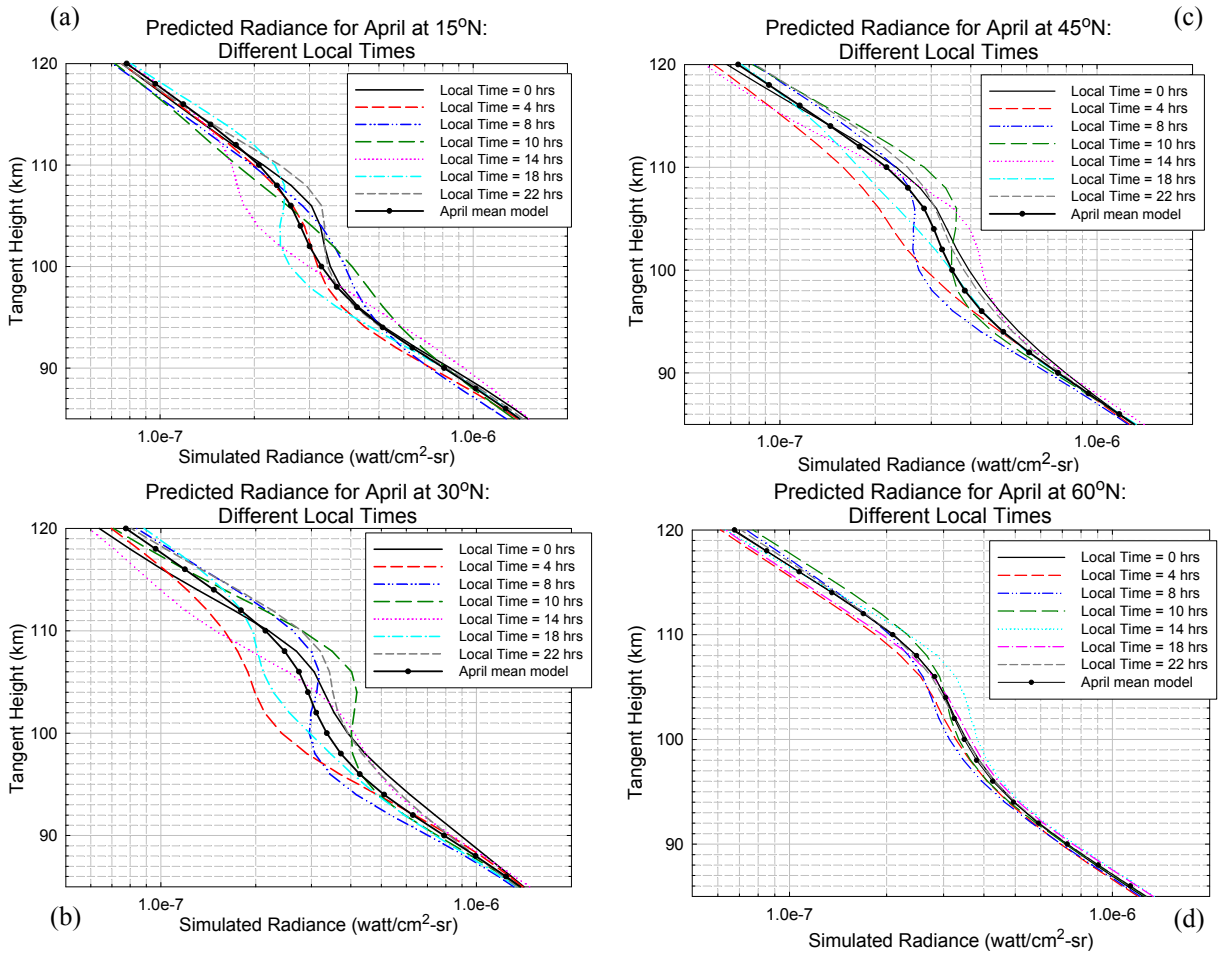

Figure 12. As Figure 11, but for four other latitudes. (a) 15°N; (b) 30°N; (c) 45°N; (d) 60°N.

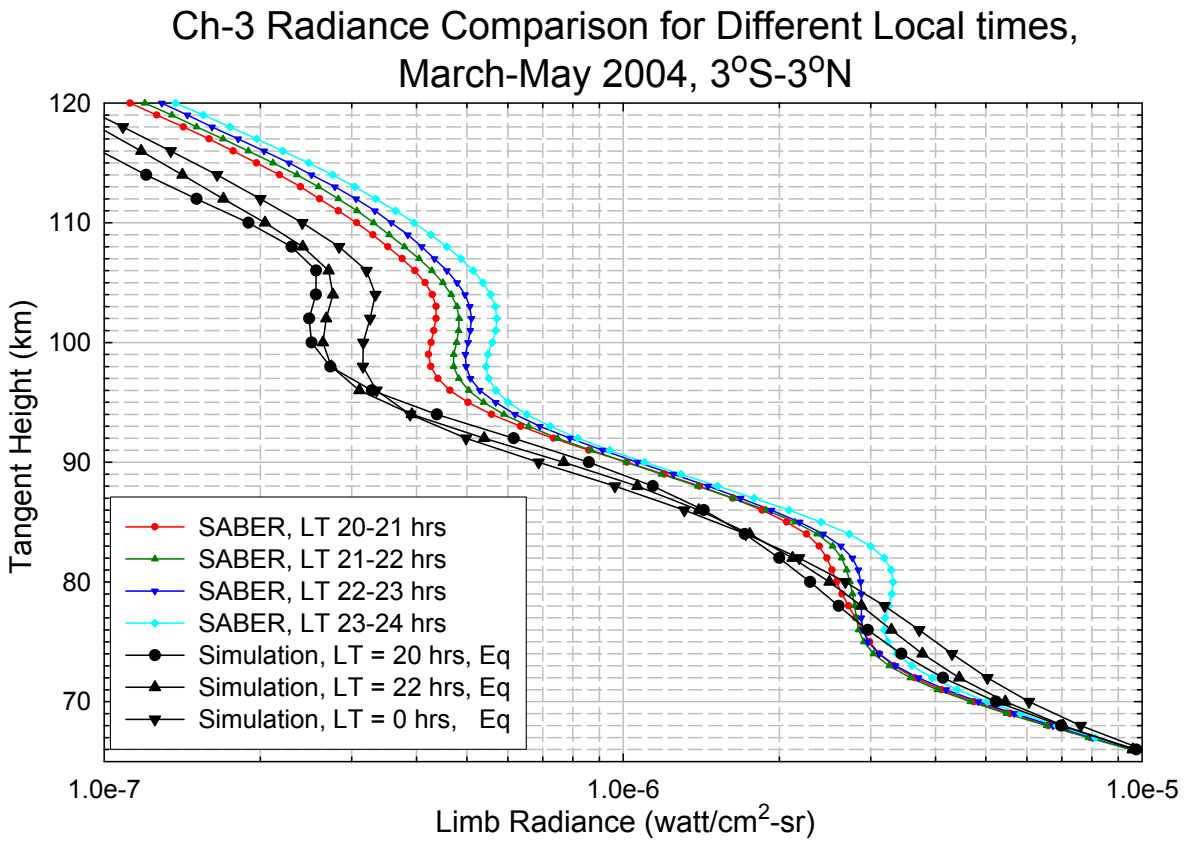

Figure 13. Comparison of SABER mean radiance with model predictions for the equatorial region, for local times in the late evening after vernal equinox. See text for discussion. The acquisition dates for the four data curves range from mid-April (LT 20-21) to late March (LT 23-24).

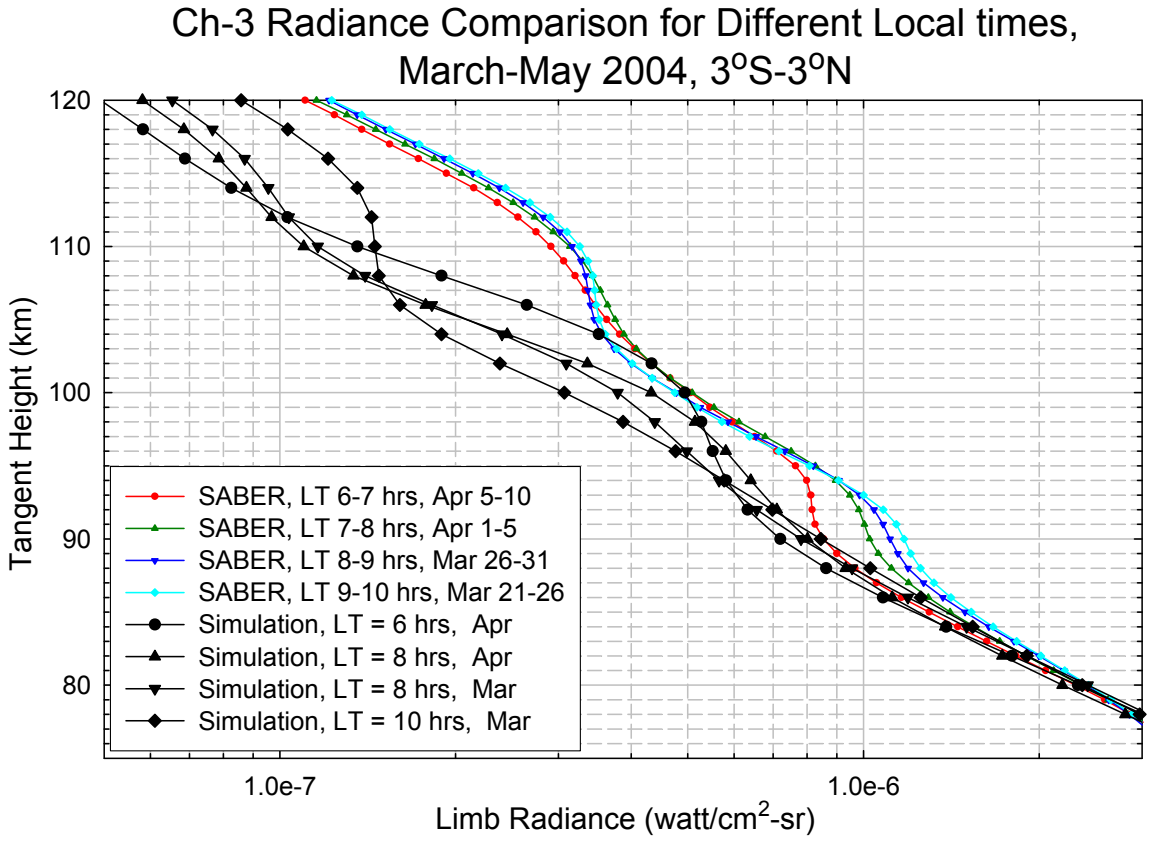

Figure 14. As Figure 13, but for prenoon local times. Data acquisition dates are given in the caption.

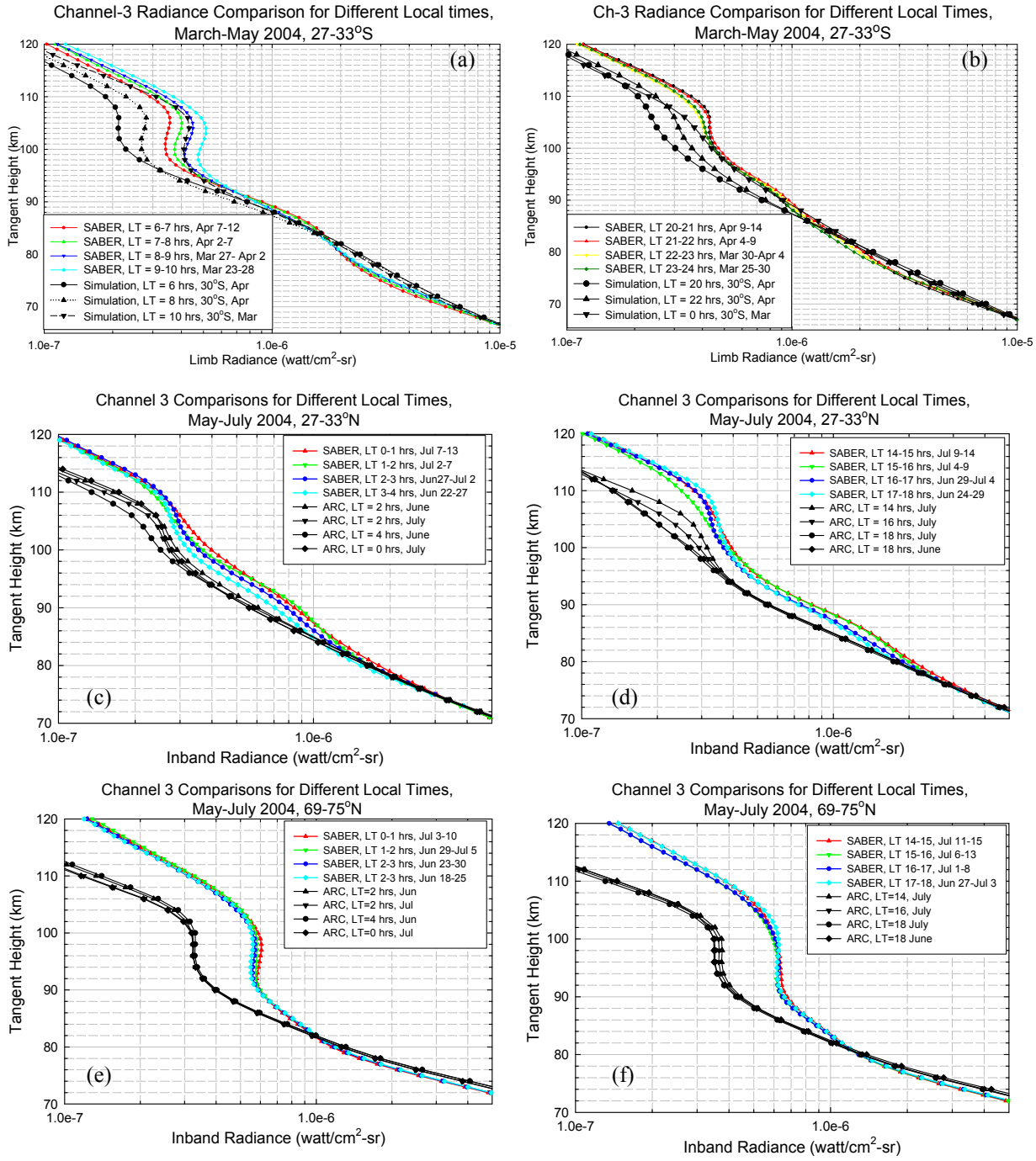

Figure 15. As Figure 13, but for various seasons, latitudes, and local times. See text for discussion.

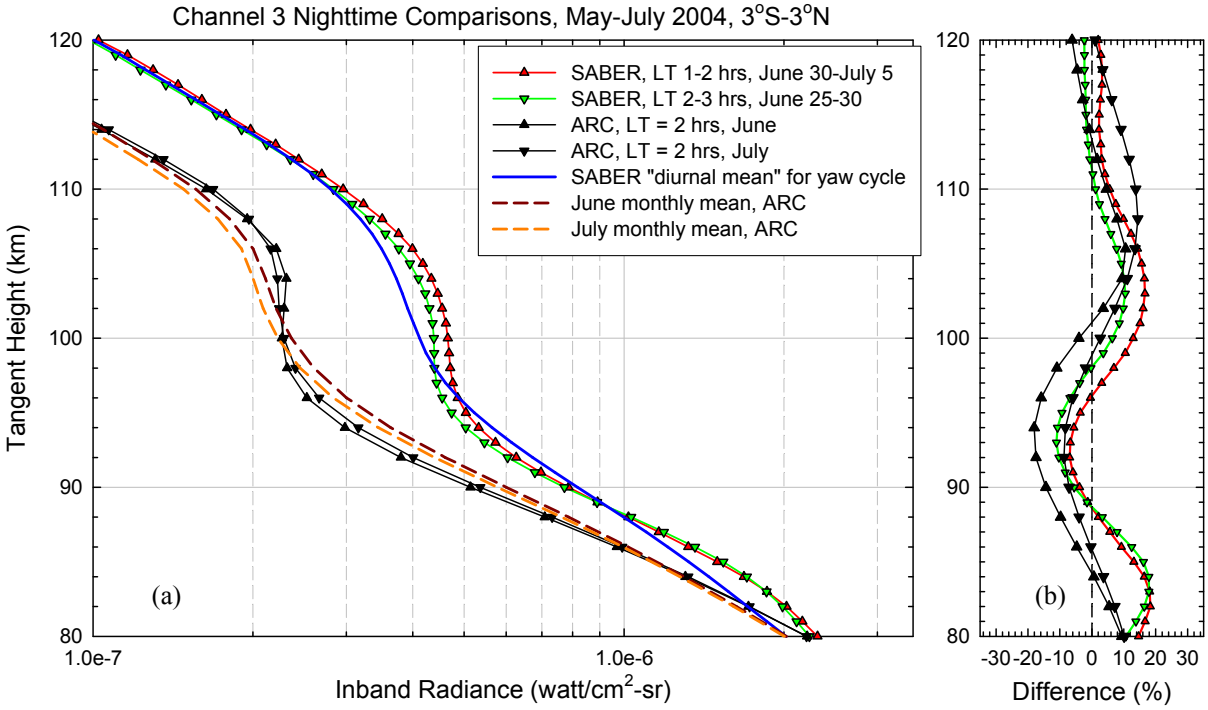

Figure 16. Model-data radiance comparison for late June/early July at the equator. (a) zonal mean profiles from SABER and ARC, plus model results and data for LT~2 hrs; (b) percent deviations of the individual profiles from their respective zonal means.

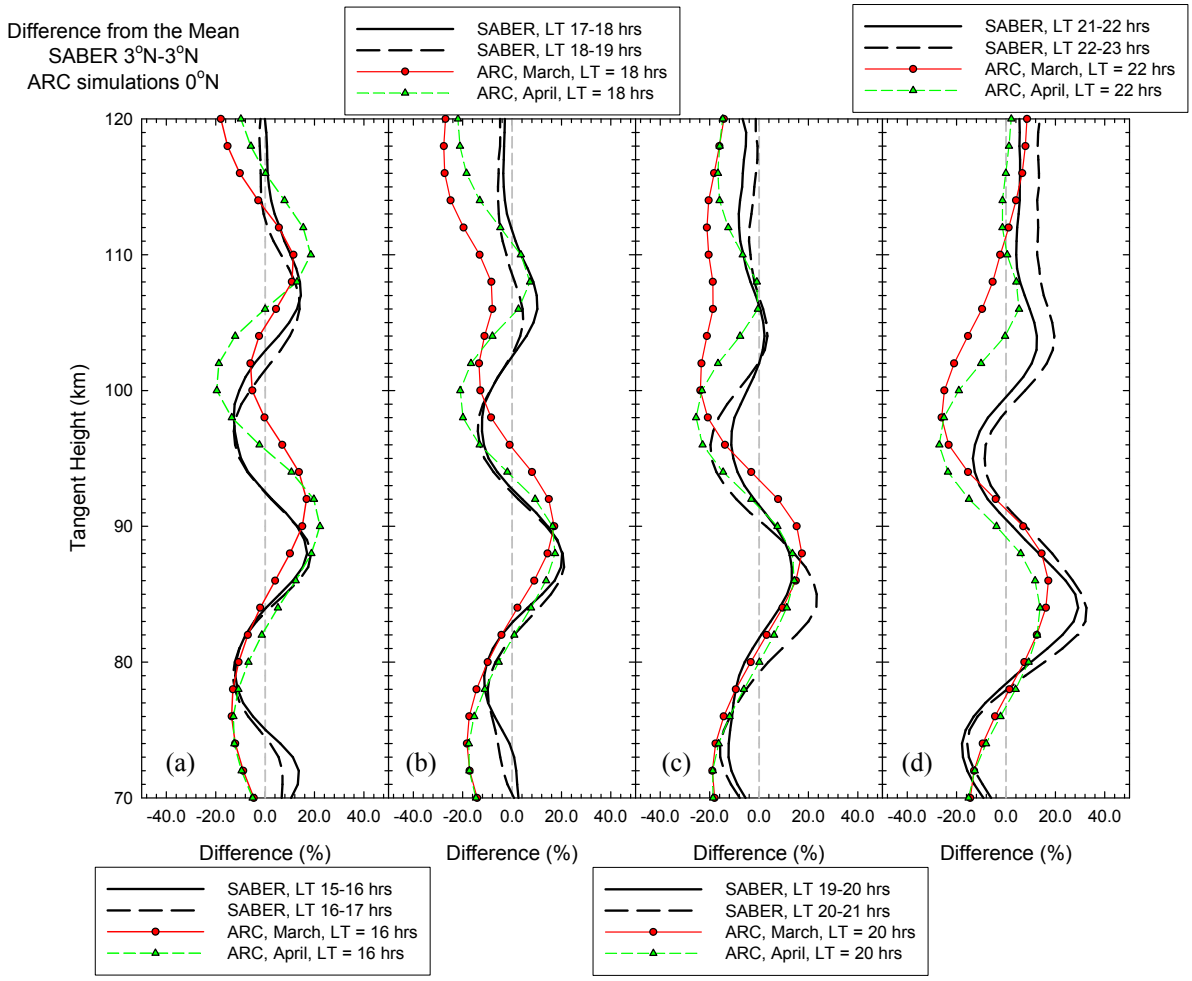

Figure 17. As Figure 16b, but for March and April at various local times. (a) LT~16 hrs; (b) LT~18 hrs; (c) LT~20 hrs; (d) LT~22 hrs.